Bezuayehu Teshome, Stefan Facsko, Adrian Keller

Topography-controlled alignment of DNA origami nanotubes on nanopatterned surfaces

Erstveröffentlichung in / First published in:
Nanoscale. 2014, 6(3), S. 1790–1796 [Zugriff am: 04.11.2019]. Royal Society of Chemistry. ISSN 2040-3372.

DOI: https://doi.org/10.1039/c3nr04627c

Nanoscale

PAPER

View Article Online
View Journal | View Issue

Cite this: *Nanoscale*, 2014, **6**, 1790

Topography-controlled alignment of DNA origami nanotubes on nanopatterned surfaces†

Bezuayehu Teshome,[ab] Stefan Facsko[a] and Adrian Keller*[a]

Received 30th August 2013
Accepted 24th November 2013

DOI: 10.1039/c3nr04627c

www.rsc.org/nanoscale

The controlled positioning of DNA nanostructures on technologically relevant surfaces represents a major goal along the route toward the full-scale integration of DNA-based materials into nanoelectronic and sensor devices. Previous attempts to arrange DNA nanostructures into defined arrays mostly relied on top-down lithographic patterning techniques combined with chemical surface functionalization. Here we combine two bottom-up techniques for nanostructure fabrication, *i.e.*, self-organized nanopattern formation and DNA origami self-assembly, in order to demonstrate the electrostatic self-alignment of DNA nanotubes on topographically patterned silicon surfaces. Self-organized nanoscale ripple patterns with periodicities ranging from 20 nm to 50 nm are fabricated by low-energy ion irradiation and serve as substrates for DNA origami adsorption. Electrostatic interactions with the charged surface oxide during adsorption direct the DNA origami nanotubes to the ripple valleys and align them parallel to the ripples. By optimizing the pattern dimensions and the Debye length of the adsorption buffer, we obtain an alignment yield of ~70%. Since this novel and versatile approach does not rely on any chemical functionalization of the surface or the DNA nanotubes, it can be applied to virtually any substrate material and any top-down or bottom-up nanopatterning technique. This technique thus may enable the wafer-scale fabrication of ordered arrays of functional DNA-based nanowires.

Introduction

DNA exhibits unique self-assembly capabilities based on Watson–Crick base pairing that can be exploited in order to create well-defined artificial DNA nanostructures with varying degrees of complexity.[1–4] Especially the DNA origami technique[4] in which a long, single-stranded DNA scaffold is folded into a predefined shape upon hybridization with a large number of short synthetic staple strands has attracted considerable attention from various research fields.[5] By this technique, it has become possible to generate complex 2D and 3D DNA nanostructures with any desired shape.[4,6–9] Among the large variety of DNA origami shapes, quasi-one dimensional DNA nanostructures hold great promise as scaffolds for nanoelectronic device fabrication as they can be used as templates to produce linear and branched metallic nanowires[10–14] and to precisely assemble metal nanoparticles[15] and semiconductor quantum dots[16] with approximately 6 nm resolution. However, the fabrication of functional devices from such DNA nanostructure templates requires their controlled arrangement and orientation on a conventional substrate.

In the past, various techniques have been employed to control the alignment of immobilized DNA nanostructures on different surfaces,[17–24] mostly by top-down lithographic patterning techniques.[17–19,21,22,24] For instance, Gerdon *et al.* have shown that by functionalizing a lithographically patterned gold surface with a carboxylic acid-terminated self-assembled monolayer, DNA origami can be selectively immobilized.[17] In a similar manner, Kershner *et al.* used electron-beam lithography (EBL) to pattern trimethylsilyl monolayers and diamond-like carbon films for the selective adsorption of DNA origami nanostructures.[18] Ding *et al.* on the other hand employed thiol-modified DNA origami nanotubes to interconnect EBL-fabricated gold islands,[19] whereas Yun *et al.* utilized chemically modified graphene as a substrate for lithographic patterning and DNA origami immobilization.[21] Most of these approaches have indeed shown great potential for the controlled alignment and orientation of DNA origami nanostructures on the surface. However, all these techniques rely on lithographic prepatterning and often also a chemical functionalization of the substrate.

Here, we demonstrate a compelling alternative approach to align DNA nanotubes on topographically patterned surfaces. To this end, we combine two bottom-up techniques for nanostructure fabrication, *i.e.*, DNA origami self-assembly and self-organized nanopattern formation on silicon surfaces during ion

[a]*Institute of Ion Beam Physics and Materials Research, Helmholtz-Zentrum Dresden-Rossendorf, 01328 Dresden, Germany. E-mail: a.keller@hzdr.de*

[b]*Technische Universität Dresden, Mommsenstraße 13, 01069 Dresden, Germany*

† Electronic supplementary information (ESI) available: Analysis of DNA origami alignment, AFM zooms of individual DNA origami nanotubes on 30 nm patterns, adsorption to 20 nm and 50 nm patterns at high Mg^{2+} concentration, TEM image of a rippled Si surface, scheme of the withdrawal geometry for molecular combing, and molecular combing on 20 nm patterns, 50 nm patterns, and flat substrates. See DOI: 10.1039/c3nr04627c

irradiation,[25,26] thus avoiding the necessity of lithographic processing or chemical modifications. The self-alignment of the DNA origami nanotubes is purely driven by electrostatic interactions with the nanorippled Si/SiO_2 surface during adsorption. By optimizing the pattern dimensions and the Debye length of the adsorption buffer, we obtain an alignment yield of ~70%. Furthermore, due to electrostatic interactions, the DNA nanotubes are not only aligned along the periodic ripple pattern but also perfectly follow the pattern and even reproduce pattern defects. Since the electrostatic origin of the self-alignment supersedes any chemical surface functionalization, this approach is not restricted to nanorippled silicon surfaces but can be extended to virtually any material of choice and to any top-down or bottom-up nanopatterning technique.

Results and discussion

The DNA origami nanotubes used in the adsorption experiments of this work were six-helix bundles with a nominal length of 412 nm and a nominal diameter of 6 nm.[16] Fig. 1 shows an atomic force microscopy (AFM) height image of dried DNA origami nanotubes adsorbed to a flat Si surface with native surface oxide. The adsorbed DNA origami nanotubes are well-dispersed and randomly oriented on the surface. Although such six-helix bundles have a persistence length well beyond 2 μm which exceeds the length of the nanotube,[27] most nanotubes are bent and distorted during adsorption and subsequent drying. This is also reflected in line scan 1 in Fig. 1 which shows a reduced length of the DNA nanotube <400 nm. In addition, the adsorbed and dried nanotubes have a mean height of only about 2 nm instead of 6 nm, indicating the collapse of the tube structure due to interactions with the surface and dehydration.

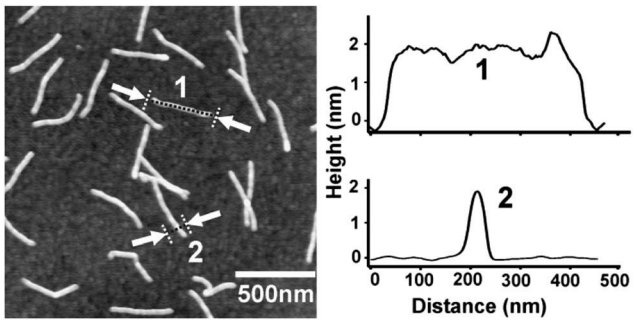

Fig. 1 AFM height image with corresponding line scans of immobilized DNA origami nanotubes on a flat Si surface. Adsorption leads to a disperse arrangement of DNA origami with random orientation. The height scale is 6 nm.

In order to investigate the influence of surface topography on the adsorption of DNA origami nanotubes, three nanopatterned substrates with varying pattern dimensions have been prepared and are characterized in Fig. 2. Well-defined periodic ripple patterns with periodicities ranging from ~20 nm to ~50 nm are observed which exhibit a well-defined quasi-sinusoidal shape. These nanoscale ripple patterns spontaneously form during off-normal low-energy ion irradiation. By varying the ion energy, the pattern periodicity can be precisely tuned in the range from <20 nm to several hundred nanometers while keeping a constant aspect ratio of ~0.1.[25] Due to their strong anisotropy, such nanopatterned substrates allow for the controlled alignment and orientation of colloidal nanospheres,[28] plasmonic nanoparticles[29] and nanowires,[30] and even cells.[31]

Fig. 3 depicts AFM topography and phase images of DNA origami nanotubes adsorbed to the three nanopatterned substrates. Due to their comparable heights, individual DNA origami nanotubes on the ripple patterns are difficult to identify in the topography images (upper row of Fig. 3). AFM phase imaging (middle row of Fig. 3), on the other hand, enables the distinction of DNA nanotubes and rippled Si due to its strong sensitivity toward chemical and mechanical surface properties.

For each of the three ripple patterns, a preferential alignment of the DNA origami nanotubes along the ripples is observed (see Fig. 3). This effect seems to be most pronounced for the 30 nm pattern (Fig. 3, center) as all nanotubes visible in

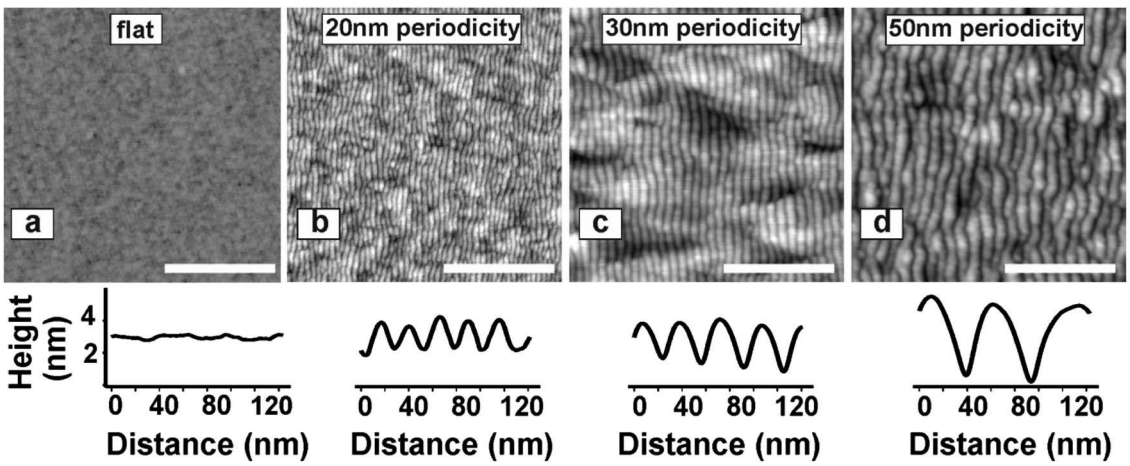

Fig. 2 AFM height images of flat (a) and nanopatterned Si surfaces (b–d). The ripple patterns have nominal periodicities of 20 nm (b), 30 nm (c), and 50 nm (d). The scale bars are 400 nm and the height scales 3 nm (a) and 6 nm (b–d). Below the AFM images, representative line scans are shown.

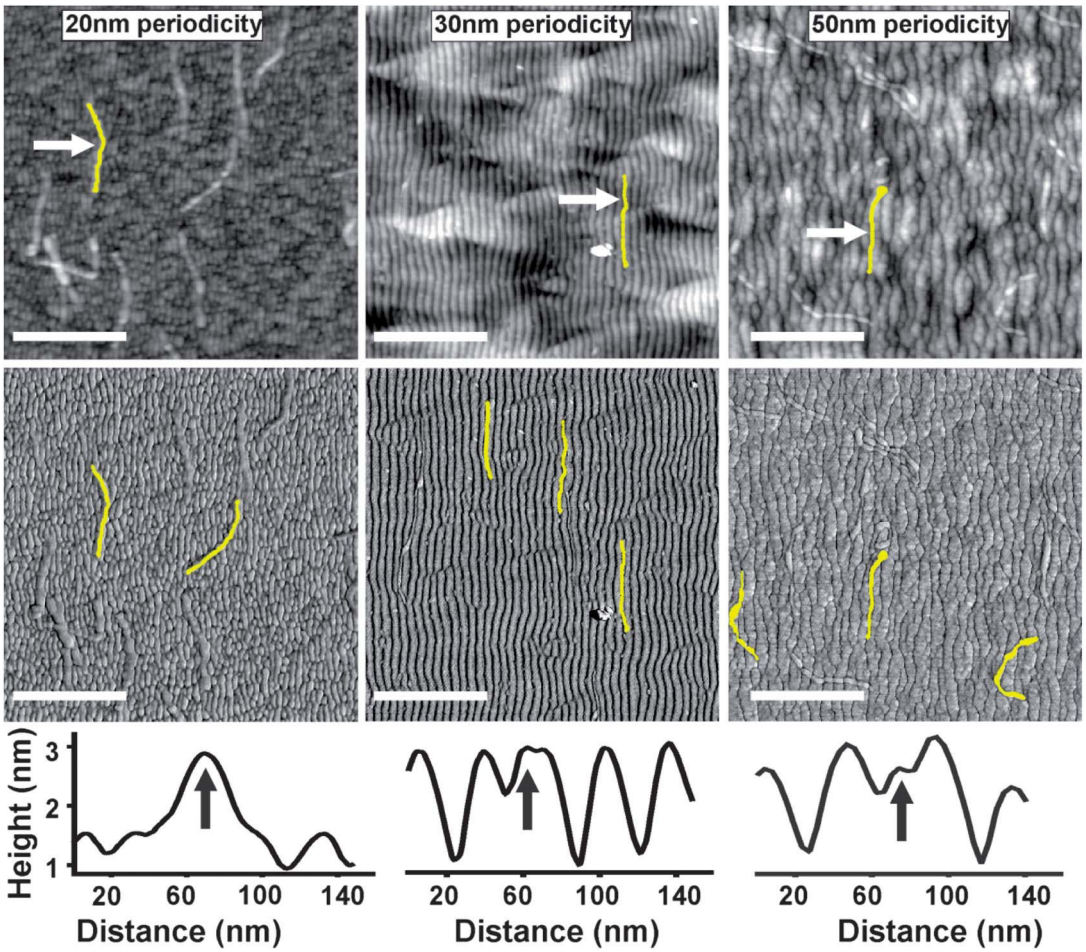

Fig. 3 AFM height (top row) and corresponding phase images (middle row) of DNA origami nanotubes adsorbed to nanopatterned Si surfaces. Some DNA origami nanotubes have been highlighted. The scale bars are 500 nm. The topographic line scans (bottom row) have been taken perpendicular to the ripples at the positions marked in the topography images. The black arrows indicate the positions of individual DNA origami nanotubes.

the corresponding AFM image appear to be located in the ripple valleys where they perfectly follow the pattern and even reproduce occasional pattern defects (see also the AFM zooms in Fig. S2†). The corresponding topographic line scan reveals that the adsorbed DNA origami nanotubes and the ripples have almost identical vertical dimensions. For the 50 nm pattern (Fig. 3, right), however, a large fraction of DNA origami nanotubes is partially located in the ripple valleys but does not closely follow the pattern while others appear to be deposited randomly. For the 20 nm pattern (Fig. 3, left), on the other hand, the DNA origami nanotubes are rather lying on top of the shallower pattern and cross between individual ripples although a certain degree of alignment is observed.

This topography effect is also reflected in the statistical distributions of the nanotube alignment shown in Fig. 4 for which between 80 and 255 DNA origami nanotubes have been analyzed. For the flat Si surface, a random orientation of the nanotubes is observed with no distinguished direction dominating. On the nanopatterned substrates with 20 nm and 50 nm periodicity, however, an alignment yield, *i.e.*, the percentage of DNA origami nanotubes aligned within $\pm 10^{\circ}$ with respect to the ripple direction, of 30.0% and 28.8%, respectively, is obtained. For the pattern with 30 nm periodicity, the alignment yield increases to 69.6%.

The flat and nanopatterned Si surfaces used in above experiments exhibit a native surface oxide of a few nanometer thickness. Under our buffer conditions, *i.e.*, at pH 8.3, the surface oxide is negatively charged.[18] Therefore, adsorption of the negatively charged DNA origami nanotubes is enabled by a high concentration (200 mM) of divalent Mg ions in the buffer which induces a charge inversion of the Si/SiO_2 surface. The alignment of the DNA origami nanotubes on the nanopatterned substrates is thus most likely driven by electrostatic interactions between the DNA origami and the surface.

In order to test this hypothesis, we have varied the $MgCl_2$ concentration during adsorption of DNA origami nanotubes to ripple patterns with 30 nm periodicity. Fig. 5 shows the determined alignment yields for three different Mg^{2+} concentrations, *i.e.*, 100 mM, 200 mM, and 500 mM. For 100 mM and 200 mM Mg^{2+}, almost identical alignment yields ~70% are obtained. However, at a higher Mg^{2+} concentration of 500 mM, the alignment yield is reduced to half this value, *i.e.*, ~36%. For the

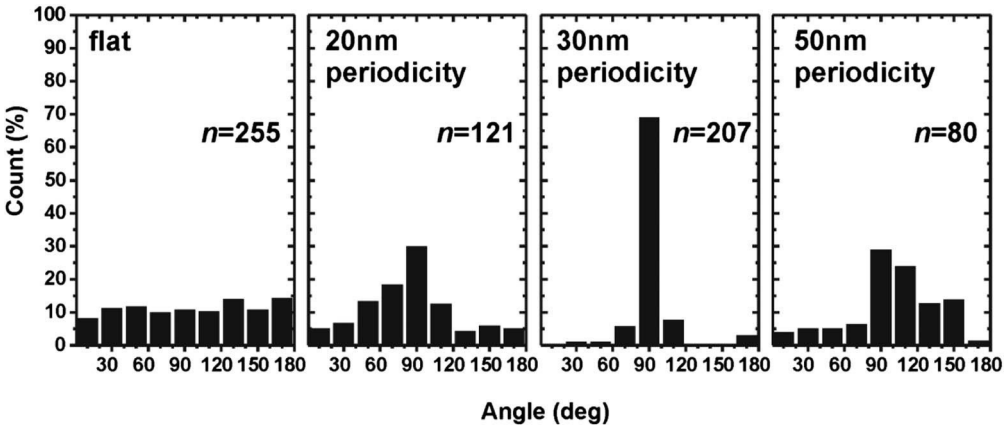

Fig. 4 Angular distribution of DNA origami nanotubes adsorbed to the different substrates. An angle of 90° corresponds to the DNA origami nanotubes being oriented parallel to the ripple pattern (see the ESI for details†). The number *n* of DNA origami nanotubes counted for each individual analysis is given in the respective plots.

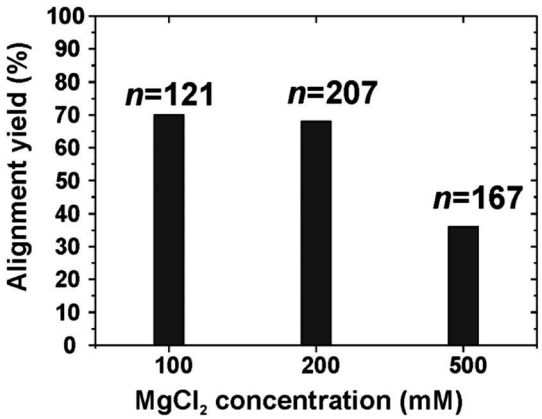

Fig. 5 Alignment yield of DNA origami nanotubes adsorbed to 30 nm ripple patterns in dependence of $MgCl_2$ concentration. The number *n* of DNA origami nanotubes counted for each individual analysis is given in the plot.

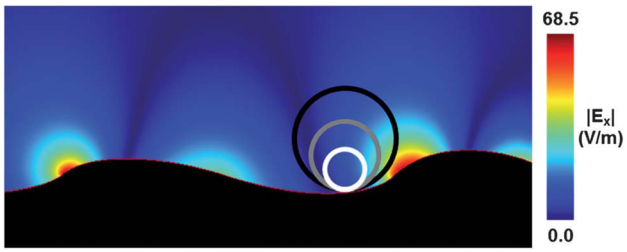

Fig. 6 Absolute values of the electric field component in the horizontal direction originating from a charged ripple surface (indicated in red) as obtained from finite element simulations. The circles represent DNA origami nanotubes adsorbed to a ripple valley. The diameter of the nanotubes (6 nm) has been scaled with respect to the ripple periodicities of 20 nm (black circle), 30 nm (grey circle) and 50 nm (white circle).

other ripple periodicities, increasing the Mg^{2+} concentration lead to random adsorption with no visible alignment (see Fig. S3†).

The increase of the Mg^{2+} concentration leads to a reduction of the Debye length of the buffer and thus to a decrease of the electrostatic forces experienced by the DNA origami during adsorption. In line with the above hypothesis, the reduction of the Debye length is accompanied by a decrease of the alignment yield of the DNA origami nanotubes. We therefore conclude that the alignment of the DNA origami nanotubes on the topographically patterned substrates is induced by the interplay between surface topography, the dimensions of the DNA nanotubes, and the Debye length of the buffer.

In order to elucidate the astonishingly strong dependence of the alignment yield on the ripple periodicity, we have performed finite element simulations of the electric fields along the rippled surface. As can be seen in Fig. 6, the charged ripple surfaces exhibit horizontal field components which guide the adsorbed yet mobile nanotubes toward the ripple slopes. Due to the slightly asymmetric shape of the ripples (see Fig. S4†), the DNA origami nanotubes will be directed preferentially toward the steeper slope. Indeed, a closer inspection of the line scans in Fig. 3 reveals that the aligned DNA origami nanotubes are always located on the right side of the ripple valleys corresponding to the steeper slope which is always facing the incoming ion beam.[32] The circles in Fig. 6 represent DNA origami nanotubes adsorbed to a ripple valley. The diameter of the nanotubes has been scaled with respect to the ripple periodicity, *i.e.*, an increasing ripple periodicity corresponds to a decreasing nanotube diameter. Obviously, DNA nanotubes adsorbed on ripple patterns with smaller periodicity experience stronger attractive fields than nanotubes on larger patterns. Therefore, the electrostatic force that directs the adsorbed nanotubes along the surface toward the steeper slope becomes weaker with increasing periodicity which is reflected in the lower alignment yield on the 50 nm ripple pattern. Although the electrostatic forces guiding the DNA nanotubes to the ripple slopes should be the strongest for the 20 nm ripple pattern, this effect is counteracted by the reduced ripple height of only ~2 nm (see Fig. 2b) which is significantly lower than the nominal diameter of the DNA origami nanotubes in solution

(6 nm) and comparable to the measured height of the dried nanotubes after adsorption (see Fig. 1). Therefore, these small-height ripples do not provide sufficient lateral confinement of the DNA origami nanotubes to single ripple valleys which consequently cross several ripple crests as can be seen in Fig. 3. This again results in a lower alignment yield.

It is well known that double-stranded DNA can be aligned along a certain substrate direction by applying a receding meniscus moving across the substrate surface, a technique called molecular combing.[33,34] In combination with lithographically patterned substrates, this method was also used to create ordered arrays of micron-long DNA nanotubes.[24] In our experiments, after incubating the DNA origami-containing buffer solution on the Si substrates, the samples were immersed in a mixture of ethanol and water which is essential for the immobilization of DNA origami on SiO_2 surfaces.[35,36] The water removes residual salt from the surface while the addition of ethanol lowers the solvation state of the Mg^{2+}-coordinated DNA origami and thereby attaches them more firmly to the oxide surface.[36] In the previous experiments, the samples were withdrawn perpendicular to the substrate surface to avoid any disturbance of the adsorbed DNA origami nanotubes (see Fig. S5†). However, in order to evaluate the influence of a possible molecular combing effect, we have varied the direction of withdrawal from the ethanol–water mixture. Therefore, samples with 30 nm periodicity have been withdrawn in two additional directions, *i.e.*, parallel and perpendicular to the orientation of the ripples as indicated in Fig. S5† and the inset of Fig. 7.

The histograms shown in Fig. 7 give the angular distributions of the adsorbed DNA origami nanotubes for the three different directions of withdrawal. Withdrawal of the sample parallel to the ripple pattern resulted in a slight reduction of the alignment yield by less than 10%. However, when the sample was withdrawn perpendicular to the pattern, the final alignment yield dropped from ~70% to ~37%. For ripple patterns with 20 nm and 50 nm periodicity, only a small reduction of the already rather low alignment yield is observed (see Fig. S6†).

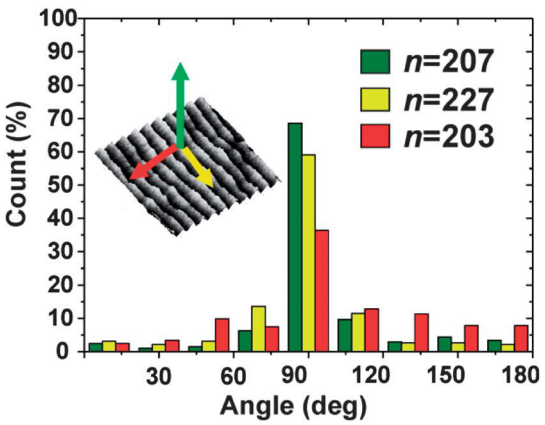

Fig. 7 Angular distribution of DNA origami nanotubes on 30 nm ripple patterns for the three different withdrawal directions indicated in the inset. The number *n* of DNA origami nanotubes counted for each individual analysis is given in the plot. The $MgCl_2$ concentration was 200 mM.

These results indicate that once-adsorbed DNA origami molecules can to a certain extent be dislocated from their original position on the sample surface by molecular combing. However, even on flat substrates, no parallel alignment of the DNA origami nanotubes due to molecular combing as reported for double-stranded DNA[33,34] has been observed (see Fig. S7†). This may be attributed to the rod-like nature of the nanotubes and possibly also to the high salt concentration of the adsorption buffer.[34] Rather, molecular combing seems to lead to a reduction of the alignment yield due to random dislocation of the already aligned DNA origami nanotubes. Therefore, care has to be taken to avoid any disturbance of the once-adsorbed DNA origami nanotubes in order to obtain maximum alignment.

Conclusions

In summary, we have shown that quasi-one dimensional DNA origami nanotubes can be aligned on topographically patterned substrates without the need for a chemical functionalization of either the substrate or the DNA origami. The self-alignment of the DNA nanotubes on shallow nanorippled Si/SiO_2 substrates is purely driven by electrostatic interactions during adsorption which direct the nanotubes toward the steeper slope of the ripples where they follow the ripple valleys. The degree of alignment is determined by the dimensions of the nanopatterns, the dimensions of the nanotubes, and the Debye length of the adsorption buffer. For a ripple pattern with 30 nm periodicity, we obtain an alignment yield of ~70% for DNA six-helix bundles in buffer containing 100–200 mM Mg^{2+}.

This novel approach may enable the wafer-scale fabrication of ordered arrays of functional DNA-based nanowires as it is not restricted to ion-induced nanopatterns but can be applied to any top-down or bottom-up nanopatterning technique such as electrochemical lithography[37] or pattern formation during semiconductor epitaxy.[38] In particular, since the alignment is purely controlled by topography, we expect that by this approach DNA origami nanotubes can also be arranged in more complex arrays by employing for instance electron beam lithography patterning or focused ion beam direct writing. In this way, complex two-dimensional, non-periodic arrangements of DNA origami nanotubes including circuit architectures for nanoelectronics could be realized. Furthermore, since the DNA origami nanotubes were found to perfectly follow the ripple valleys even around pattern defects, also arrangements of curved DNA nanotubes may be generated with such techniques. Nevertheless, self-organized nanopattern formation during low-energy ion irradiation is a well-established, highly parallel, and versatile technique that can be applied to a large variety of technologically relevant materials including other semiconductors, metals, and insulators.[26] We therefore believe that the combination of these two bottom-up techniques, *i.e.*, ion-induced nanopattern formation and DNA origami self-assembly, will contribute to the full-scale integration of functional DNA-based materials into technological devices.

Methods

The design of the DNA origami six-helix bundles was adopted from Bui *et al.*[16] DNA origami assembly was performed by mixing the M13mp18 viral DNA scaffold (5 nM) with 170 staple strands in a 1 : 30 molar ratio in TAE buffer containing 20 mM Mg^{2+} (Sigma-Aldrich) in a total volume of 100 μL. The solution was then heated to 80 °C and cooled in 90 min to 4 °C in an Eppendorf Mastercycler Personal machine. Excess staple strands were removed by spin filtering the sample two times for 10 min at 6000 rpm after addition of 300 μL TAE/Mg^{2+} with an Amicon Ultra-0.5 mL filter with 100 kDa MWCO (Millipore). M13mp18 viral DNA and staple strands were purchased from New England Biolabs and Metabion, respectively.

Commercially available epi-polished p-Si(100) wafers with native surface oxide were used as substrates for adsorption. Off-normal ion irradiation was performed at room temperature as previously described using a Kaufman ion source (Ar^+ irradiation) and a low-energy ion implanter (Xe^+ irradiation).[32,39] The irradiation parameters for the individual samples are given in Table 1.

Immediately before DNA origami adsorption, the flat and nanopatterned substrates (100 mm^2 area) were cleaned in oxygen plasma for 3 min and subsequently rinsed with ethanol and Milli-Q water. Adsorption of the DNA origami was performed in a humidity chamber by incubating a 2 μL aliquot of the DNA origami sample in 60 μL of 10× TAE/Mg^{2+} buffer on the Si substrate. After 1 h, the Si substrate with the DNA origami-containing buffer solution was removed from the humidity chamber and immediately dipped in a 1 : 1 mixture of ethanol and Milli-Q water for 30 seconds to remove residual salt from the surface and dehydrate the DNA origami. The samples were then dried in a N_2 stream oriented ~45° with respect to the ripple direction.

The adsorbed DNA origami was imaged and characterized by tapping mode AFM in air using a MultiMode 8 scanning probe microscope (Bruker) and PPP-NCLR cantilevers from Nanosensors (nominal force constant 48 N m^{-1}, tip radius <10 nm). The histograms of the orientation of the DNA origami on the different substrates have been determined from 6 to 12 AFM images taken at different positions on the surface of each substrate. The orientation of the DNA origami with respect to the ripple structure was analyzed using Gwyddion open source software[40] (see the ESI for details†).

The electric field above the rippled Si/SiO_2 surface was calculated using the program COMSOL Multiphysics (Version 3.2) to solve the Poisson's equation with the finite element method. Two regions were defined in the two-dimensional electrostatics module: the silicon substrate with an isotropic $\varepsilon = 12.1$ as the bottom sub-domain and water with $\varepsilon = 1$ as the top sub-domain, respectively. On the boundary between the sub-domains, which mimics the real ripple surface, a homogeneous surface charge density of 1×10^{-9} C m^{-2} was applied. The top boundary of the domain was set to ground potential whereas the other boundaries of the domain were set to "zero charge/symmetry".

Table 1 Periodicities and irradiation parameters of the nanorippled substrates used in this work

Periodicity (nm)	Ion	Energy (keV)	Incident angle (deg)	Fluence (cm^{-2})
21.5 ± 1.0	Ar^+	0.3	67	8×10^{17}
32.5 ± 2.5	Ar^+	0.5	67	8×10^{17}
50.8 ± 2.0	Xe^+	5	65	2×10^{17}

Acknowledgements

We thank I. Winkler for performing the Xe^+ irradiation and I. Bald for a careful reading of the manuscript. This work was kindly supported by the Deutsche Forschungsgemeinschaft (FOR845) and the Initiative and Networking Fund of the Helmholtz Association of German Research Centers through the International Helmholtz Research School for Nanoelectronic Networks, IHRS NANONET (VH-KO-606).

Notes and references

1 N. C. Seeman, *J. Theor. Biol.*, 1982, **99**, 237–247.
2 E. Winfree, F. Liu, L. A. Wenzler and N. C. Seeman, *Nature*, 1998, **394**, 539–544.
3 W. M. Shih, J. D. Quispe and G. F. Joyce, *Nature*, 2004, **427**, 618–621.
4 P. W. K. Rothemund, *Nature*, 2006, **440**, 297–302.
5 T. Tørring, N. V. Voigt, J. Nangreave, H. Yan and K. V. Gothelf, *Chem. Soc. Rev.*, 2011, **40**, 5636–5646.
6 E. S. Andersen, M. Dong, M. M. Nielsen, K. Jahn, R. Subramani, W. Mamdouh, M. M. Golas, B. Sander, H. Stark, C. L. P. Oliveira, J. S. Pedersen, V. Birkedal, F. Besenbacher, K. V. Gothelf and J. Kjems, *Nature*, 2009, **459**, 73–76.
7 S. M. Douglas, H. Dietz, T. Liedl, B. Högberg, F. Graf and W. M. Shih, *Nature*, 2009, **459**, 414–418.
8 H. Dietz, S. M. Douglas and W. M. Shih, *Science*, 2009, **325**, 725–730.
9 D. Han, S. Pal, J. Nangreave, Z. Deng, Y. Liu and H. Yan, *Science*, 2011, **332**, 342–346.
10 H. Yan, S. H. Park, G. Finkelstein, J. H. Reif and T. H. LaBean, *Science*, 2003, **301**, 1882–1884.
11 R. Schreiber, S. Kempter, S. Holler, V. Schüller, D. Schiffels, S. S. Simmel, P. C. Nickels and T. Liedl, *Small*, 2011, **7**, 1795–1799.
12 A. C. Pearson, J. Liu, E. Pound, B. Uprety, A. T. Woolley, R. C. Davis and J. N. Harb, *J. Phys. Chem. B*, 2012, **116**, 10551–10560.
13 J. Liu, Y. Geng, E. Pound, S. Gyawali, J. R. Ashton, J. Hickey, A. T. Woolley and J. N. Harb, *ACS Nano*, 2011, **5**, 2240–2247.
14 Y. Geng, A. C. Pearson, E. P. Gates, B. Uprety, R. C. Davis, J. N. Harb and A. T. Woolley, *Langmuir*, 2013, **29**, 3482–3490.
15 A. Kuzyk, R. Schreiber, Z. Fan, G. Pardatscher, E.-M. Roller, A. Högele, F. C. Simmel, A. O. Govorov and T. Liedl, *Nature*, 2012, **483**, 311–314.

16 H. Bui, C. Onodera, C. Kidwell, Y. Tan, E. Graugnard, W. Kuang, J. Lee, W. B. Knowlton, B. Yurke and W. L. Hughes, *Nano Lett.*, 2010, **10**, 3367–3372.
17 A. E. Gerdon, S. S. Oh, K. Hsieh, Y. Ke, H. Yan and H. T. Soh, *Small*, 2009, **5**, 1942–1946.
18 R. J. Kershner, L. D. Bozano, C. M. Micheel, A. M. Hung, A. R. Fornof, J. N. Cha, C. T. Rettner, M. Bersani, J. Frommer, P. W. K. Rothemund and G. M. Wallraff, *Nat. Nanotechnol.*, 2009, **4**, 557–561.
19 B. Ding, H. Wu, W. Xu, Z. Zhao, Y. Liu, H. Yu and H. Yan, *Nano Lett.*, 2010, **10**, 5065–5069.
20 A. C. Pearson, E. Pound, A. T. Woolley, M. R. Linford, J. N. Harb and R. C. Davis, *Nano Lett.*, 2011, **11**, 1981–1987.
21 J. M. Yun, K. N. Kim, J. Y. Kim, D. O. Shin, W. J. Lee, S. H. Lee, M. Lieberman and S. O. Kim, *Angew. Chem. Int. Ed.*, 2012, **51**, 912–915.
22 B. Gao, K. Sarveswaran, G. H. Bernstein and M. Lieberman, *Langmuir*, 2010, **26**, 12680–12683.
23 A. Kuzyk, B. Yurke, J. J. Toppari, V. Linko and P. Törmä, *Small*, 2008, **4**, 447–450.
24 C. Lin, Y. Ke, Y. Liu, M. Mertig, J. Gu and H. Yan, *Angew. Chem. Int. Ed.*, 2007, **46**, 6089–6092.
25 A. Keller and S. Facsko, *Materials*, 2010, **3**, 4811–4841.
26 W. L. Chan and E. Chason, *J. Appl. Phys.*, 2007, **101**, 121301.
27 T. Liedl, B. Högberg, J. Tytell, D. E. Ingber and W. M. Shih, *Nat. Nanotechnol.*, 2010, **5**, 520–524.
28 A. Mathur, A.-D. Brown and J. Erlebacher, *Langmuir*, 2006, **22**, 582–589.
29 T. W. H. Oates, A. Keller, S. Facsko and W. Möller, *Plasmonics*, 2007, **2**, 47–50.
30 B. Fazio, C. D'Andrea, F. Bonaccorso, A. Irrera, G. Calogero, C. Vasi, P. G. Gucciardi, M. Allegrini, A. Toma, D. Chiappe, C. Martella and F. Buatier de Mongeot, *ACS Nano*, 2011, **5**, 5945–5956.
31 E. J. Tocce, V. K. Smirnov, D. S. Kibalov, S. J. Liliensiek, C. J. Murphy and P. F. Nealey, *Biomaterials*, 2010, **31**, 4064–4072.
32 A. Biermanns, U. Pietsch, J. Grenzer, A. Hanisch, S. Facsko, G. Carbone and T. H. Metzger, *J. Appl. Phys.*, 2008, **104**, 044312.
33 D. Bensimon, A. J. Simon, V. Croquette and A. Bensimon, *Phys. Rev. Lett.*, 1995, **74**, 4754–4757.
34 Z. Deng and C. Mao, *Nano Lett.*, 2003, **3**, 1545–1548.
35 A. Keller, I. Bald, A. Rotaru, E. Cauet, K. V. Gothelf and F. Besenbacher, *ACS Nano*, 2012, **6**, 4392–4399.
36 A. M. Hung, C. M. Micheel, L. D. Bozano, L. W. Osterbur, G. M. Wallraff and J. N. Cha, *Nat. Nanotechnol.*, 2010, **5**, 121–126.
37 F. C. Simeone, C. Albonetti and M. Cavallini, *J. Phys. Chem. C*, 2009, **113**, 18987–18994.
38 C. Teichert, *Phys. Rep.*, 2002, **365**, 335–432.
39 A. Keller, S. Facsko and W. Möller, *New J. Phys.*, 2008, **10**, 063004.
40 D. Nečas and P. Klapetek, *Cent. Eur. J. Phys.*, 2011, **10**, 181–188.

